In Vivo Phosphorylation of Human Erythrocyte Spectrin Occurs in a Sequential Manner†

Hsin-Yao Tang and David W. Speicher*

The Wistar Institute, 3601 Spruce Street, Philadelphia, Pennsylvania 19104

Received November 21, 2003; Revised Manuscript Received February 12, 2004

ABSTRACT: Spectrin is the major component of the erythrocyte membrane skeleton and exists as a 526 kDa $\alpha\beta$ heterodimer. The 246 kDa β-chain of human spectrin is phosphorylated near the C-terminus, but the exact phosphorylation sites are unknown and the role of this phosphorylation is not fully characterized. In this study, we produced a monoclonal antibody, Sp316, capable of recognizing the C-terminal region of β-spectrin regardless of its phosphorylation state and used it to purify the phosphorylated region after 2-nitro-5-thiocyanobenzoic acid cleavage of spectrin. Two-dimensional gels, mass spectrometry, and reversed-phase high-performance liquid chromatography were used to characterize these phosphorylation states. Only about 1.5% of spectrin isolated from fresh blood is unphosphorylated, about 9% has more than four phosphates per molecule, and the majority of the protein has one to four phosphates per molecule. A total of six phosphorylation sites were identified by tandem mass spectrometry. Quantitative analysis of the phosphorylation states by reversed-phase high-performance liquid chromatography revealed that phosphorylation of β-spectrin occurs in a sequential manner where each specific site is completely phosphorylated before the next site is modified. The first phosphorylation event occurs on Ser-2114, followed by Ser-2125, Ser-2123, Ser-2128, Ser-2117, and Thr-2110. The identification of the specific phosphorylated β-spectrin residues and the ordered sequence of phosphorylation events in vivo should provide an invaluable basis for further studies of the role of these posttranslational modifications in spectrin function in situ.

The intracellular surface of the erythrocyte membrane contains a network of proteins that form the membrane skeleton. This protein skeleton is largely responsible for the unique properties of the erythrocyte membrane including its biconcave shape, elasticity, and deformability (*1*−*3*). The major component of the membrane skeleton is spectrin, which is composed of two large subunits, α (280 kDa) and β (246 kDa), that associate laterally in an antiparallel manner to form heterodimers (*4*−*6*). Both subunits primarily consist of multiple tandem homologous triple-helical motifs of about 106 amino acid residues, with 20 motifs in the α-chain and 17 in the β-chain (*4*, *5*, *7*). The N-terminus of α-spectrin (α0) consists largely of a single unpaired helix and the last homologous motif of β-spectrin (β17) has a partial motif consisting of two helices. In erythrocytes, spectrin exists predominately as tetramers that are formed by head-to-head self-association of two heterodimers. The tetramerization region involves interactions of the unpaired α0 helix with the two helices of β17 to form a complete triple-helical motif (*8*−*10*). Spectrin tetramers are crucial for maintaining the stability and integrity of the cell, and mutations that affect tetramer formation frequently result in hereditary hemolytic anemias (*11*−*18*).

Erythrocyte spectrin undergoes a number of naturally occurring or pathologically induced posttranslational modifications such as phosphorylation, carbamylation, ubiquitination, glycosylation, and oxidation (*19*−*24*). Phosphorylation is the most extensively studied covalent modification of spectrin due to its potential role in regulating spectrin function. The phosphorylation state of spectrin is dependent on various kinases and phosphatases present on the plasma membrane and in the cytoplasm of the erythrocyte (*19*, *25*−*30*). ^{32}P-labeling studies indicate that only the β-subunit of spectrin is phosphorylated in intact erythrocyte (*19*, *31*−*33*), but the functional role of this phosphorylation remains ambiguous. Early in vitro studies were not able to show any effects of phosphorylation on tetramer formation, interaction with ankyrin, or cell shape (*34*−*36*). However, in situ studies by Manno et al. (*37*) using intact erythrocyte membranes demonstrated that an increase in β-spectrin phosphorylation caused a decrease in erythrocyte membrane mechanical stability, which suggested the studies using isolated proteins did not adequately mimic interactions within intact membranes. In addition, certain leukemia patients with elliptocytosis and poikilocytosis displayed an elevated amount of spectrin dimers coinciding with increased β-spectrin phosphorylation (*38*). Both findings strongly suggest that increased phosphorylation of spectrin destabilizes tetramer formation and has important in vivo physiological functions.

The phosphorylation sites on β-spectrin were roughly mapped to the C-terminal region in an early seminal

† This work was supported in part by the National Institutes of Health Grant HL38794 to D.W.S., NCI Cancer Core Grant CA10815, and the Commonwealth Universal Research Enhancement Program, Pennsylvania Department of Health.

* To whom correspondence should be addressed: Phone (215) 898-3972; fax (215) 898-0664; e-mail speicher@wistar.upenn.edu.

10.1021/bi036092x CCC: $27.50
Published on Web 03/19/2004

structural study (*19*). It is now known from the cDNA sequence (*5*) that β-spectrin contains a terminal short nonhomologous segment with a calculated mass of 5.8 kDa located immediately after the β17 partial motif that contains the tetramer binding site. In the early spectrin phosphorylation site study, an average of four phosphates, three phosphoserines and one phosphothreonine, were localized within a 20 kDa cyanogen bromide (CNBr)[1] fragment on the extreme C-terminal end of β-spectrin (*19*). In addition, all phosphorylation sites in β-spectrin could be removed by mild tryptic proteolysis with an apparent 8 kDa reduction in molecular mass as determined by sodium dodecyl sulfate−polyacrylamide gel electrophoresis (SDS−PAGE) (*39*). On the basis of the minimum size of the identified phosphorylated region in these early studies compared with the known sequence mass, these data suggested that β-spectrin phosphorylation sites may extend into the β17 motif that is involved in tetramer formation. In support of this possibility, the elliptocytosis-associated spectrin Rouen was able to be phosphorylated despite deletion of the β-chain C-terminal nonhomologous region (*18*). In addition to the uncertainty in location of phosphorylation sites, Pedroni et al. (*40*) reported that β-spectrin may contain at least six phosphorylated residues based on the number of components they observed using two-dimensional gels. Therefore, to further dissect the functional role of β-spectrin phosphorylation, a precise analysis of the extent of β-spectrin phosphorylation in vivo, identification of the specific phosphorylated amino acids, and elucidation of the in vivo phosphorylation pattern (sequential or random) are needed.

In this report, we identified a total of six phosphorylated residues that define the phosphorylation states of spectrin in intact human red cells. Furthermore, we present evidence that phosphorylation of β-spectrin occurs in a specific ordered fashion.

MATERIALS AND METHODS

Materials. 2-Nitro-5-thiocyanobenzoic acid (NTCB) was purchased from Sigma−Aldrich (St. Louis, MO). Trypsin (sequencing grade) was obtained from Promega (Madison, WI). All other reagents were high-performance liquid chromatography (HPLC) grade or the highest quality analytical reagent grades. The monoclonal antibody (mAb) to β-spectrin nonhomologous C-terminal region (Sp316) was obtained by immunizing mice with the recombinant β16−17C peptide and was developed with the assistance of The Wistar Institute Monoclonal Antibody Core Facility. The recombinant β-spectrin expression plasmids were generated by polymerase chain reaction with Vent polymerase (New England Biolabs). The β-spectrin cDNA template was kindly provided by Dr. Bernard Forget (Yale University, New Haven, CT).

[1] Abbreviations: CNBr, cyanogen bromide; NTCB, 2-nitro-5-thiocyanobenzoic acid; RP-HPLC, reversed-phase high-performance liquid chromatography; mAb, monoclonal antibody; PCR, polymerase chain reaction; GST, glutathione S-transferase; SDS, sodium dodecyl sulfate; PAGE, polyacrylamide gel electrophoresis; EDTA, ethylenediaminetetraacetic acid; PMSF, phenylmethanesulfonyl fluoride; MOPS, 3-(*N*-morpholino)propanesulfonic acid; Tris, tris(hydroxymethyl)aminomethane; Bis-Tris, bis(2-hydroxyethyl)aminotris(hydroxymethyl)-methane; 2-DE, two-dimensional gel electrophoresis; IPG, immobilized pH gradient; MALDI, matrix-assisted laser desorption/ionization; TOF, time-of-flight; MS, mass spectrometry; MS/MS, tandem mass spectrometry; LC, liquid chromatography; IMAC, immobilized metal ion affinity chromatography; IEF, isoelectric focusing.

Isolation of Spectrin from Human Erythrocytes and Purification of Recombinant Proteins. Crude spectrin was obtained from low ionic strength extracts of human erythrocyte ghosts as previously described (*42*). The β-spectrin recombinant proteins β16−17 (Thr-1902 to Arg-2084) and β16−17C (Thr-1902 to Tyr-2137) were produced as glutathione S-transferase (GST) fusion proteins using the pGEX-2T vector (Amersham Biosciences) and GST was removed from the proteins by use of bovine thrombin (Sigma) as previously described (*43*). The cleaved recombinant proteins were purified by rechromatography on a glutathione−Sepharose column, concentrated with a Centriprep YM10 concentrator (Millipore), and further purified by gel filtration on a HiLoad 16/60 Superdex 75 column (Amersham Biosciences).

NTCB Cleavage of Cysteine Residues and Sp316 mAb Purification of NTCB Peptides. Crude spectrin extract or β16−17C (dialyzed in 1 mM sodium phosphate, 0.5 mM EDTA, 0.5 mM β-mercaptoethanol, and 0.15 mM PMSF, pH 7.5) were lyophilized and redissolved in 200 mM Tris-HCl, 6 M guanidine hydrochloride, and 1 mM EDTA, pH 8.0, at a final concentration of 2 mg/mL. NTCB was then added in 20-fold molar excess of the total cysteine content. The cyanylation reaction was allowed to proceed for 1 h at 37 °C, after which the pH of the reaction was raised to 9.0 with 1 M NaOH for cleavage to occur (*44*). In some experiments, prior to the pH increase, the reaction mixture was chromatographed on an Econo-Pac 10DG column (Bio-Rad) equilibrated with 20 mM Tris-HCl, 6 M guanidine hydrochloride, and 1 mM EDTA, pH 8.0, to prevent artifactual carbamylation caused by NTCB reaction byproducts. The reaction was stopped after 16 h of incubation at 37 °C by adding β-mercaptoethanol to a final concentration of 3 mM. Gel analysis of the NTCB reaction products was performed after dialysis in 20 mM NH_4HCO_3 and 1 mM β-mercaptoethanol, pH 8.0.

For antibody binding, the quenched NTCB reaction mixture was diluted 6-fold with 20 mM Tris-HCl, 130 mM NaCl, and 0.1% Triton X-100, pH 7.0, and applied onto a column containing Sp316 mAb coupled to CNBr-activated Sepharose CL-4B beads at 4 °C. After the column was washed with the same buffer, the bound NTCB peptides were eluted with 100 mM triethylamine and 0.1% IGEPAL CA-630 (Sigma), pH 11.5, and neutralized with $^1/_{10}$ volume of 2 M Tris-HCl, pH 6.0. Fractions containing NTCB peptides were pooled, dialyzed against 20 mM NH_4HCO_3 and 1 mM β-mercaptoethanol, pH 8.0, and lyophilized. For dephosphorylation reactions, lyophilized samples were dissolved in 0.01% SDS, and an aliquot was treated with 2 units of shrimp alkaline phosphatase (Roche Diagnostics) at 37 °C for 30 min in the buffer supplied by the manufacturer.

Polyacrylamide Gel Electrophoresis and Western Blot Analysis. 1-D SDS gels were performed using 6% Tris-glycine Laemmli gels (*45*) or 12% NuPAGE Bis-Tris gel with MOPS running buffer (Invitrogen) as indicated. For Western blots, proteins separated by 1-D gels were blotted onto Immobilon P membranes (Millipore) as described previously (*42*). The primary antibody was Sp316 mAb, and the secondary antibody was horseradish peroxidase-conjugated anti-mouse IgG (Promega). The enhanced chemiluminescence Western blotting detection reagents (Amersham

Biosciences) were used to visualize antibody−antigen interactions.

For 2-D polyacrylamide gel electrophoresis (2-DE), lyophilized samples were dissolved in 7 M urea, 2 M thiourea, 0.1 M dithiothreitol, 2% IGEPAL CA-630, and 2% IPG buffer, pH 4−7. Proteins were isoelectrofocused by use of pH 4−7 immobilized pH gradient (IPG) strips (18 cm) on the IPGphor isoelectric focusing system (Amersham Biosciences). The strips were rehydrated and focused by a 10 h rehydration (1 h without current, 9 h at 30 V) followed by 1 h each at 500, 1000, and 2000 V, followed by 8000 V for a total of 45 kV·h. Immediately prior to loading focused strips on the second-dimensional gels, the strips were reduced and alkylated as described previously (*46*). Second-dimensional gels were performed on Tris−glycine SDS−13% polyacrylamide gels (*45*) prepared in Bio-Rad vertical Protean II xi chambers (18 × 18 cm, 1.5 mm thickness) and were stained with Coomassie Brilliant Blue R-250 or Colloidal Blue (Invitrogen). Stained 2-D gels were analyzed after densitometry scanning by use of Melanie 3 2-DE analysis software (Genebio, Geneva, Switzerland).

Tryptic Digest and Reversed-Phase HPLC Separation of Peptides. Protein spots were subjected to in-gel tryptic digestion as previously described (*47*). Tryptic peptides were separated by reversed-phase (RP) HPLC on a Zorbax 300SB−C18 column (2.1 × 150 mm 5-micron, Agilent) using a Beckman Coulter System Gold 126 system (Beckman Instruments, Fullerton, CA) at a flow rate of 0.2 mL/min. Solvent A was 0.05% trifluoroacetic acid (TFA) in Milli-Q water, and solvent B was 0.045% TFA in 95% acetonitrile. The peptides were eluted with a gradient program consisting of 0% B for 5 min, 0−5% B over 5 min, 5−25% B over 65 min, 25−45% B over 50 min, 45−75% B over 15 min, and 75% B for 10 min. The absorbance was monitored at 215 nm.

Mass Spectrometric Analyses. Masses were obtained by matrix-assisted laser desorption/ionization time-of-flight-mass spectrometry (MALDI-TOF MS) on a Voyager DE-PRO mass spectrometer (Perspective Biosystems). Samples were desalted by use of C18 Ziptips (Millipore) when necessary. Peptides were applied to MS sample plates precoated with a saturated solution of nitrocellulose and α-cyano-4-hydroxycinnamic acid (1:4 w/w) in 2-propanol/acetone (50:50 v/v) (*48*). For β16−17C, the protein solution was diluted 1:1 with a saturated solution of sinapinic acid in 33% acetonitrile and 0.1% TFA.

Tandem mass spectrometry (MS/MS) of tryptic peptides was performed on an LCQ ion trap mass spectrometer (Thermo Electron). Tryptic peptides were separated with a C18 reversed-phase capillary column (75 μm i.d. × 10 cm) as described previously (*46*). The LCQ was set to repetitively monitor *m*/*z* of 400−1800, executing data-dependent scans on the most abundant ions, followed by high-resolution zoom scans and MS/MS. In some experiments, to increase sensitivity for detection of low-abundance phosphopeptides, the instrument was set to monitor specific *m*/*z* corresponding to the phosphorylated peptides, followed directly by MS/MS fragmentations.

Immobilized Metal Ion Affinity Chromatography Purification of Phosphorylated Peptides. In some experiments, phosphopeptides from tryptic digests were isolated by use of ZipTip pipet tips (Millipore). The IMAC tips were washed with 0.1% acetic acid/50% acetonitrile; charged with 200 mM $GaCl_3$; washed with Milli-Q water followed by 1% acetic acid/10% acetonitrile; and equilibrated with 0.1% acetic acid/10% acetonitrile. Tryptic digests were acidified with 20% acetic acid (1:1 ratio) and loaded onto the IMAC tips. The tips were then washed with 0.1% acetic acid/10% acetonitrile followed by Milli-Q water. The bound peptides were eluted with 200 mM sodium phosphate, pH 8.9, desalted by use of C18 ZipTips (Millipore), and analyzed by MALDI MS.

RESULTS

Immunoaffinity Purification of the β-Spectrin Phosphorylated Region with Sp316 mAb. To facilitate the study of the β-spectrin phosphorylation sites, we produced a mAb capable of recognizing the C-terminal region of β-spectrin regardless of its phosphorylation state. This mAb, Sp316, recognized β-spectrin specifically from crude spectrin prepared from low ionic strength extracts of human erythrocyte ghosts (Figure 1A). The Sp316 mAb was also able to recognize a recombinant fragment (β16−17C) containing the 16th and 17th repeats and the nonhomologous C-terminal region (Figure 1B, lane 5). But the antibody did not recognize β16−17, which lacks the nonhomologous region (Figure 1B, lane 6). Furthermore, the nonhomologous C-terminal region of β-spectrin is highly susceptible to proteolysis (*6*) and the purified recombinant β16−17C displayed a number of degradation products that did not interact with the Sp316 mAb (Figure 1B, lane 5). MALDI MS analysis of the purified β16−17C showed that the intact protein mass (MH^+) of 27 473.45 Da was within experimental error of the calculated mass of 27 477.76 Da (Figure 1C). The largest degradation product of β16−17C that did not bind to Sp316 has a MH^+ of 26 028.18 (Figure 1C), indicating that the epitope for Sp316 is located within the last 12 amino acids of β-spectrin.

To isolate the phosphorylated region, spectrin was cleaved with NTCB and peptides containing the C-terminus were purified with the Sp316 antibody column (Figure 1B, lanes 1 and 2). NTCB cleaves cysteine residues but the reaction is usually highly incomplete, presumably due to a competing β-elimination reaction (*44*). Hence, multiple protein bands with apparent molecular masses ranging from about 17 to 120 kDa were observed due to cleavage at cysteine residues at different distances from the C-terminus of β-spectrin. The apparent 17 kDa peptide represents the C-terminal 127 residues of β-spectrin resulting from cleavage at Cys-2012, and the abundant apparent 21 kDa peptide is produced by cleavage at Cys-1962 (Figure 2). The multiple bands between the 17 and 21 kDa bands were due to artifactual migration of 17 kDa peptides with differing phosphorylation levels (Figure 1B, lane 2). On lower percentage acrylamide gels, the 21 kDa band can also be resolved into phosphorylation-related multiple bands (data not shown). Dephosphorylation of these peptides with alkaline phosphatase collapsed the multiple bands between 17 and 21 kDa to a single band with similar mobility to the NTCB fragment from unphosphorylated Sp316-purified β16−17C (Figure 1B, lanes 3 and 4).

Analysis of Sp316-Purified Spectrin NTCB Peptides by High-Resolution 2-DE. 2-DE is useful for separating different

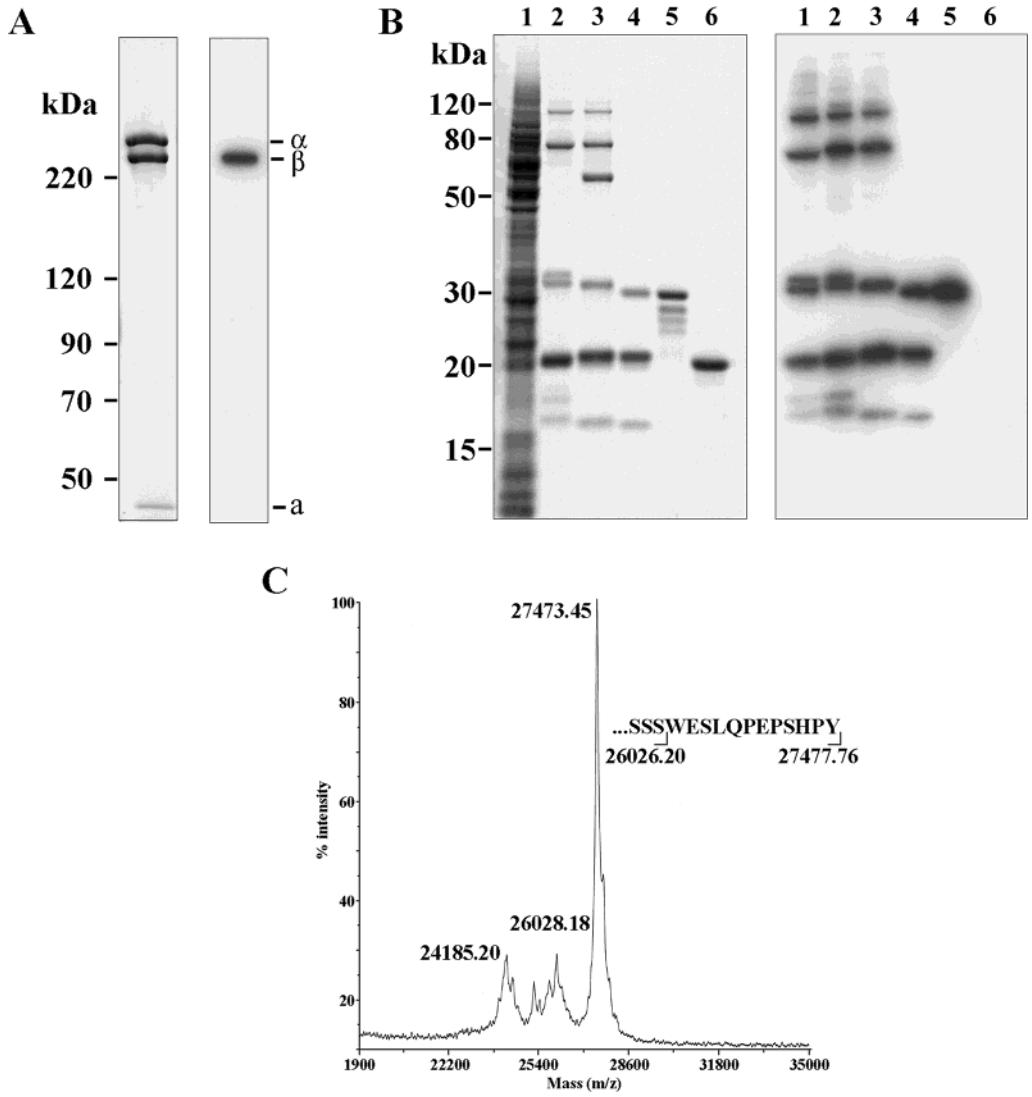

FIGURE 1: Characterization of the Sp316 mAb and affinity purification of β-spectrin phosphorylated region. (A) Spectrin extract separated on 6% Tris−glycine SDS−polyacrylamide gel stained with Coomassie Blue (left) and western blot of a replicate gel (right) probed with the Sp316 mAb. α and β indicate α- and β-spectrin; a indicates actin. (B) NTCB cleavage of spectrin extract (lane 1), Sp316 mAb-purified spectrin NTCB peptides without (lane 2) and with (lane 3) alkaline phosphatase treatment, Sp316-purified β16−17C NTCB peptides (lane 4), uncleaved β16−17C (lane 5), and uncleaved β16−17 (lane 6) electrophoresed on 12% NuPAGE Bis-Tris gel with MOPS running buffer, stained with Colloidal Blue (left) and western blot of a replicate gel (right) probed with the Sp316 mAb. (C) MALDI MS spectrum of β16−17C. Average masses (MH^+) of the three major peaks and the C-terminal sequence of β16−17C with calculated masses are shown.

phosphorylation states of proteins (*49*). We (*6*) and Pedroni et al. (*40*) previously reported the separation of ^{32}P-labeled spectrin NTCB peptides by 2-D gels. However, the peptides were poorly resolved by older 2-D gel methods, and no attempt was made to characterize them. In this study, we initially used a similar NTCB cleavage condition to that used in previous studies (*6*, *40*), but we found a significant amount of the NTCB fragments (up to 45%) were carbamylated on lysine residues (data not shown). These unexpected artifactual modifications resulted in isoelectric point shifts similar to those caused by phosphorylation, but we were able to minimize the carbamylation artifact by subjecting the cyanylated reaction mixture to gel filtration before the overnight cleavage at 37 °C.

With the improved NTCB cleavage method, Sp316-purified spectrin NTCB peptides displayed increased yield of larger fragments due to reduced efficiency of the NTCB cleavage. When analyzed on high-resolution 2-D gels, nine spots (charge states) were observed for the 21 and 32 kDa peptides, whereas four major spots were observed for the 17 kDa peptide (Figure 3A,B). Some of the spots have a corresponding faster migrating species. The positions of the unphosphorylated fragments (P0) were determined by use of Sp316-purified NTCB peptides of the unphosphorylated recombinant β16−17C cleaved under identical conditions (Figure 3C). Two-dimensional gel analysis of the unphosphorylated β16−17C NTCB peptides mixed with spectrin NTCB peptides unequivocally identified the P0 position for the 17 and 21 kDa series (Figure 3D). Since addition of phosphates will cause acidic shifts of the peptides, the eight spots more acidic than P0 suggest the presence of up to eight phosphorylation sites in β-spectrin. Most of the peptides have one to four phosphates, and a minor amount have zero or more than four phosphates (Figure 3B). For the 21 kDa series, the most abundant phosphorylation state is P2 (33.0%), followed by P3 (26.6%), P1 (15.5%), P4 (14.1%), P5 (4.5%), P6 (2.8%), P0 (1.5%), P7 (1.4%), and finally P8 (0.6%). A similar distribution of phosphorylation states was

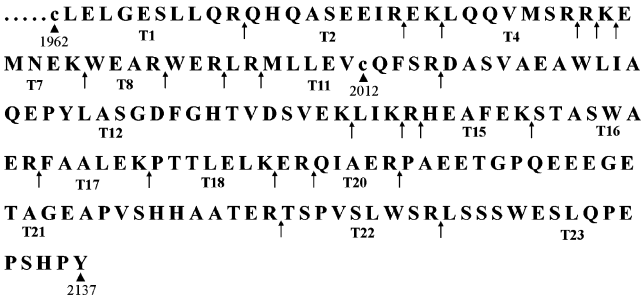

FIGURE 2: Amino acid sequence of the 21 kDa β-spectrin NTCB peptide. The two cysteine residues (lower case) and numerical positions of the cysteine residues and the terminal tyrosine residue in the complete sequence of β-spectrin (*5*) are shown. Arrows indicate trypsin cleavage sites, and major tryptic peptides are labeled. For T12, cleavage was also observed after Tyr-2031, resulting in T12.1 (Asp-2017 to Tyr-2031) and T12.2 (Leu-2032 to Lys-2046). The nonhomologous C-terminal region of β-spectrin begins at approximately Pro-2085 (beginning of T21).

observed for the 17 kDa peptides, except that the unphosphorylated peptide and peptides with more than four phosphate groups were not clearly visible, presumably due to the lower amount of peptides in this series. Also, the SDS gel migration artifact caused by phosphorylation is much more pronounced on the 17 kDa peptides than on larger peptides (Figures 1B and 3A).

Analysis of the unphosphorylated β16−17C NTCB peptides containing the C-terminal region revealed a minor amount of charge heterogeneity (Figure 3C). About 16% of the total peptide displayed a one-charge acidic shift, and 5% had a two-charge shift. The nature of these shifts is not known but is not caused by the carbamylation artifact observed when reaction mixtures were not desalted prior to incubation at pH 9.0 (data not shown). While no distinct spot was observed in the basic region, a minor smear (~5%) of the peptide was apparent. It is likely that similar nonphosphate charge heterogeneity will occur for the spectrin peptides and will be superimposed on the phosphorylation-related shifts. In addition, about 10% of the unphosphorylated peptide appeared to migrate faster. This is most likely caused by proteolysis of the parent peptide. Faster migrating species were also observed in spectrin peptides at P2 in 32 kDa, P1 in 21 kDa, and in P2 and P3 of the 17 kDa peptides.

RP-HPLC Tryptic Peptide Maps of the β-Spectrin 21 kDa NTCB Peptides. Although all peptides on the 2-D gel (Figure 3A) contained the β-spectrin C-terminal region, the most useful peptides for peptide mapping were the 21 kDa series, since their yields were higher than the 17 kDa fragments and the different charge states were adequately separated. All spots in the 21 kDa series were excised, digested in-gel with trypsin, and analyzed by RP-HPLC (Figure 4). Due to the low yields of P0, P7 and P8, high-quality reliable comparative maps could not be generated for these peptides. A reference P0 map was obtained from the major spot of the recombinant β16−17C 21 kDa NTCB peptide (Figure 3C). The identity of each peak was determined by MALDI MS (Table 1), and peaks showing differences in retention time or abundance were confirmed by tandem MS or Edman sequencing. The numbering and sequence of each tryptic peptide are shown in Figure 2. Except for T11, all other tryptic peptides containing serine or threonine were recovered (Table 1). Comparison of the RP-HPLC maps to the P0 map shows that, in P1, there is a clear loss of the T22 peptide and appearance of a new peak containing the singly-phosphorylated T22 (T22P). In P2, loss of T23 and appearance of the singly-phosphorylated T23 (T23P) were observed. In P3 and P4, the T23P peak disappeared but no major new peaks emerged. For P5 and P6, a major loss of T22P and reduction of T21 (compare T21 and T16) were observed. In

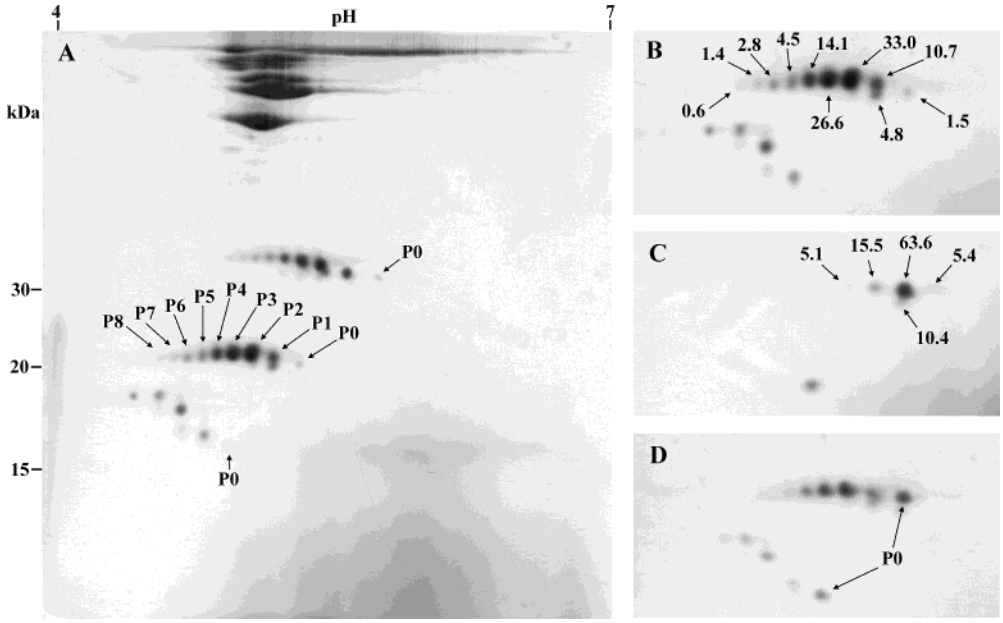

FIGURE 3: Analysis of the phosphorylated C-terminal region of spectrin by 2-DE. (A) Sp316 mAb-purified NTCB peptides of spectrin extract. Crude spectrin was cleaved with NTCB and the C-terminal region was purified on an Sp316 antibody column. The different charge states of the 21 kDa peptides are indicated (isolated from 3.2 mg of crude spectrin). P0 refers to the unphosphorylated state. (B) Expanded view of the same gel showing the 17 and 21 kDa peptides. (C, D) Expanded view of gels showing the 17 and 21 kDa Sp316-purified NTCB peptides of β16−17C (94 μg, panel C), and spectrin/β16−17C mixture (isolated from 1.6 mg of crude spectrin and 47 μg of β16−17C, panel D). The numbers in B and C refer to the percentage of each 21 kDa spots. All samples were focused on pH 4−7 IPG strips, followed by separation on Tris−glycine SDS−13% polyacrylamide gels. Proteins were visualized by staining with Colloidal Blue.

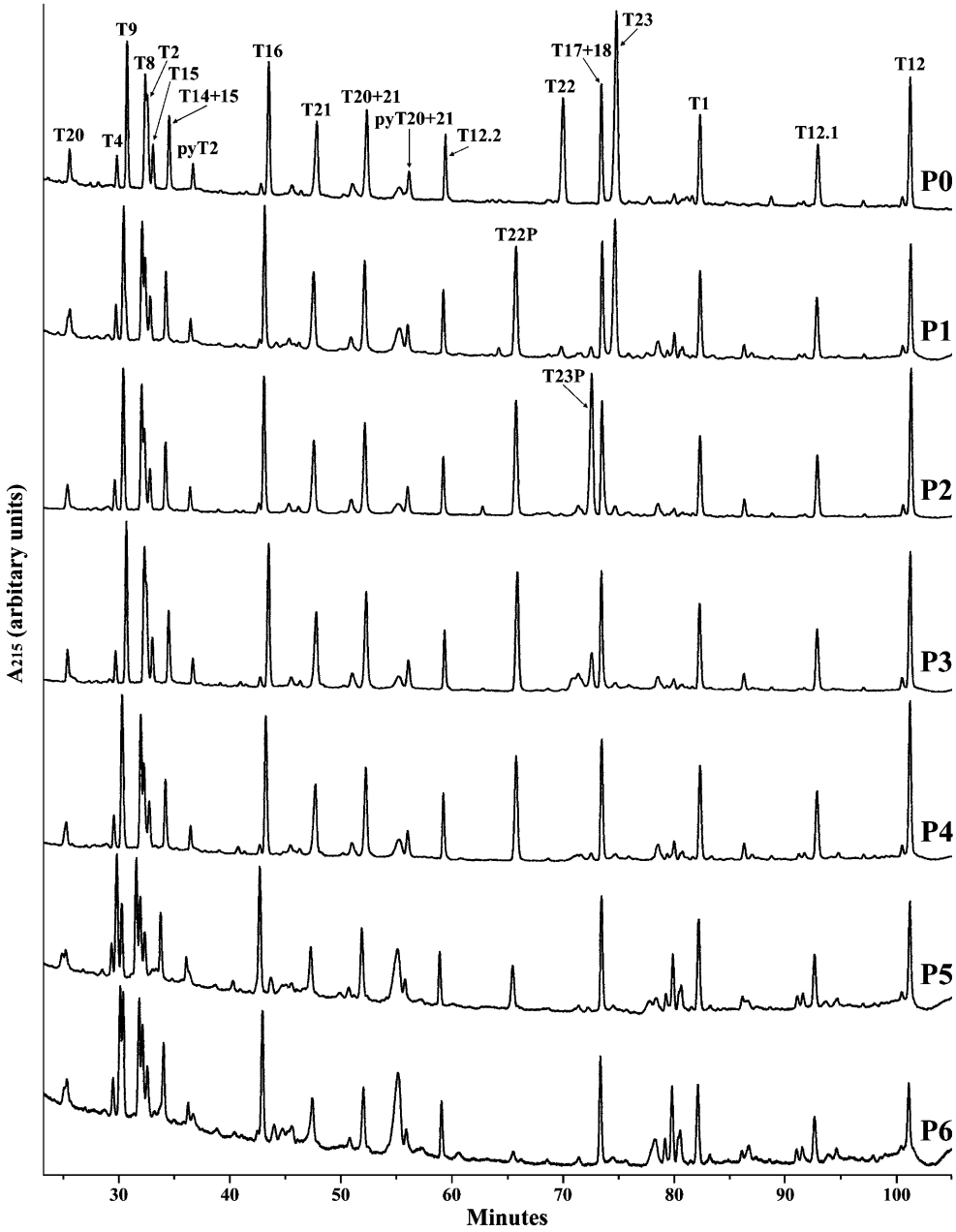

FIGURE 4: Comparative RP-HPLC tryptic peptide maps of the 21 kDa NTCB peptides. The P1−P6 spots of the 21 kDa spectrin NTCB peptides were excised, in-gel digested with trypsin, and analyzed by RP-HPLC. The P0 map was obtained from the major 21 kDa spot of recombinant β16−17C cleaved with NTCB. The faster migrating species of P1 was not included in the P1 tryptic digest. The identities of all major peaks are shown. pyT2 and pyT20+21 indicate peptides where the N-terminal Gln residue was converted to pyroglutamic acid during the trypsin digestion.

addition, the T12 peak also decreased in P5 and P6, but similar reduction in T12 was also observed in RP-HPLC tryptic maps of unphosphorylated β16−17C displaying the acidic charge shifts (Figure 3C; data not shown). This suggests that T12 had undergone a nonphosphate modification resulting in decreased yield of the T12 peak. The nature of this modification is unknown. All other spectrin tryptic peptide-containing peaks did not show significant changes and, aside from T22P and T23P peaks, no other peaks containing phosphorylated peptides were recovered.

These results indicate that phosphorylation occurs in a sequential fashion. The first phosphorylation event occurs on T22 and the second on T23. While no further peaks containing phosphorylated peptides were recovered, the clear loss of T23P in P3 and P4 suggests the third and fourth phosphorylation events are due to addition of a second and third phosphate on T23P, respectively. A minor heterogeneity of phosphorylation states was observed but was consistent with the extent of acidic shift caused by the nonphosphorylation charge heterogeneity observed in the NTCB peptide from the recombinant β16−17C (Figure 3C).

Since phosphorylation of T23 is the second phosphorylation event, the contribution of the non-phosphate charge shifts can be estimated from the amount of T23P in P1 and P3/P4. On the basis of RP-HPLC integrated peak areas, the percentages of T23P in P1 (basic shift), P2 (no shift), P3 (single acid shift), and P4 (double acid shifts) are 5.2%, 74.5%, 16.6%, and 3.7%, respectively. This is in good agreement with the amount of charge heterogeneity determined from 2-D gel analysis of β16−17C (Figure 3C). The

Table 1: MALDI MS Analysis of the RP-HPLC Fractions of P0 Tryptic Digest[a]

tryptic peptide	calcd mass (MH^+)	obsd mass (MH^+)	tryptic peptide	calcd mass (MH^+)	obsd mass (MH^+)
T1	1285.68[b]	1286.37	T16	907.43	907.16
T2	1097.53	1097.95	T17+18	1460.85	1460.69
pyT2	1080.53[c]	1080.78	T20	616.34	616.44
T4	861.46	877.85[d]	T21	2916.29	2914.69
T8	561.28	561.47	T20+21	3513.63	3512.25
T9	490.24	490.44	pyT20+21	3496.63[c]	3497.74
T12.1	1662.79	1684.48[e]	T22	1032.55	1032.35
T12.2	1561.74	1561.39	T22P	1112.55	1112.52
T12	3205.53	3204.82	T23	1843.85	1843.66
T15	760.36	760.46	T23P	1923.85	1924.13
T14+15	916.48	916.47			

[a] The masses shown are monoisotopic masses, obtained in the reflector mode with delayed extraction. The phosphorylated peptides T22P and T23P were obtained from P1 and P2 tryptic digests, respectively. [b] After NTCB cleavage, the peptide mass increased by 25 Da due to formation of 2-iminothiazolidine from cysteine (*44*). [c] Conversion of Gln to pyroglutamic acid (py) reduced the mass by 17 Da. [d] The Met oxidized (+16 Da) mass was observed. [e] The sodium adduct (+22 Da) of this peptide was observed.

maps of P5 and P6 suggest the next two phosphorylation events occur on T22P and T21. Taking into account the non-phosphate charge shifts and the large difference in the amounts of P3/P4 and P5 (Figure 3B), a substantial amount of P3/P4 is expected to comigrate in the P5 spot due to the acidic shifts. Similarly, the P6 spot would contain some amount of P4 and P5. Since the peak area of T21 and T22P in P5 is 63% and 42% of that in P4, respectively, the predominant phosphorylation event in P5 is the double phosphorylation of T22P.

MALDI MS Analysis of the β-Spectrin 21 kDa NTCB Peptides. While RP-HPLC mapping of tryptic peptides is able to provide quantitative assessments of the relative yields of each peptide, its usefulness is limited in this study by the inability to recover tryptic peptides with multiple phosphates from the reversed-phase column, presumably due to irreversible binding of these peptides to metal surfaces of the HPLC components and/or heterogeneous interaction with the column. To verify the specific peptides modified at higher phosphorylation states, we analyzed the tryptic digest mixtures of 21 kDa spots by MALDI MS without separation. For maximum sensitivity, masses were obtained in linear mode. In agreement with the RP-HPLC mapping, T22 and T23 phosphorylations were found to occur in P1 and P2, respectively (Figure 5). In P3, a new peak corresponding to the mass of doubly phosphorylated T23 (T23PP) was observed as predicted by interpretation of the RP-HPLC chromatograms. This peak was greatly reduced in P4, and a new peak with the mass of triply phosphorylated T23 (T23PPP) was detected. Each successive phosphorylation of T23 reduced the ionization efficiency of these peptides, as would be expected for addition of strongly negatively charged groups. In P5 and P6, the mass spectra were similar to that of P4 and no new peaks corresponding to other phosphorylated peptides were detected (data not shown). To confirm that these peptides were phosphorylated, we used IMAC ZipTips to selectively enrich phosphorylated peptides from tryptic digests (*50*). When the tryptic digests were subjected to IMAC analysis, all the phosphorylated peptides identified by MALDI MS of the unfractionated tryptic digests were isolated by the IMAC tip. The isolation of the four phosphorylated peptides of the P4 tryptic digest by IMAC is shown in Figure 5. Not surprisingly, peptides with stretches of acidic residues, such as T21, were isolated as well. IMAC analysis of P5 and P6 tryptic digests did not yield additional phosphorylated peptides (data not shown). Therefore, MALDI MS analysis was successful in identifying four phosphorylated peptides and confirmed that the phosphorylation events on P3 and P4 were caused by double and triple phosphorylation of T23, respectively (Table 2).

Identification of Phosphorylated Residues by LC-MS/MS. In the experiments described above, all the phosphorylation events were localized to the T22 and T23 tryptic peptides. Both peptides have multiple serine or threonine residues that could potentially be phosphorylated (Figure 2). To identify the exact phosphorylation sites and other phosphorylation events not found by MALDI MS, the tryptic digests of β-spectrin 21 kDa NTCB peptides were analyzed by LC-MS/MS. MS/MS spectra were compared to the theoretical spectra of tryptic peptides by use of SEQUEST, allowing for possible covalent addition of a phosphate molecule (80 Da increase) to Ser and Thr, and all identified sites were manually verified. Representative MS/MS spectra showing the specific residue modified by each phosphorylation event are shown in Figure 6. For example, in P1, MS/MS fragmentation of a doubly charged ion at *m*/*z* 556.87 generated a mixture of b- and y-series fragment ions that corresponded to T22P (Figure 6). A dominant fragment ion (*m*/*z* 508.0) that is 49 Da less than the parent ion was observed, corresponding to the neutral loss of H_3PO_4, which is a hallmark of phosphopeptides subjected to fragmentation in ion trap mass spectrometers (*51*, *52*). In addition, fragment ions containing the phosphorylated residues have the tendency to partially lose H_3PO_4 through β-elimination, converting phosphoserine to dehydroalanine and phosphothreonine to dehydroaminobutyric acid (*51*, *52*). The appearance of b2 and b4 ions, having an 80 Da increase to their calculated mass, indicates either Thr-2113 or Ser-2114 was

Table 2: Summary of the Phosphorylation Events and Identification of the Phosphorylated Residues in the C-Terminal Region of β-Spectrin

phosphorylation event	tryptic peptide	calcd mass (MH^+)		obsd mass (MH^+)		phosphorylated residues[a]
		no phosphate	phosphorylated	MALDI-MS	LC-MS/MS	
P1	T22P	1032.55	1112.55	1112.25	1112.74	TS*PVSLWSR
P2	T23P	1843.85	1923.85	1923.86	1923.90	LSSS*WESLQPEPSHPY
P3	T23PP	1843.85	2003.85	2003.92	2004.26	LS*SS*WESLQPEPSHPY
P4	T23PPP	1843.85	2083.85	2083.63	2083.80	LS*SS*WES*LQPEPSHPY
P5	T22PP	1032.55	1192.55		1192.56	TS*PVS*LWSR
P6	T21P	2916.29	2996.29		2996.29	PAEETGPQ...SHHAAT*ER

[a] Asterisks indicate phosphorylated residues.

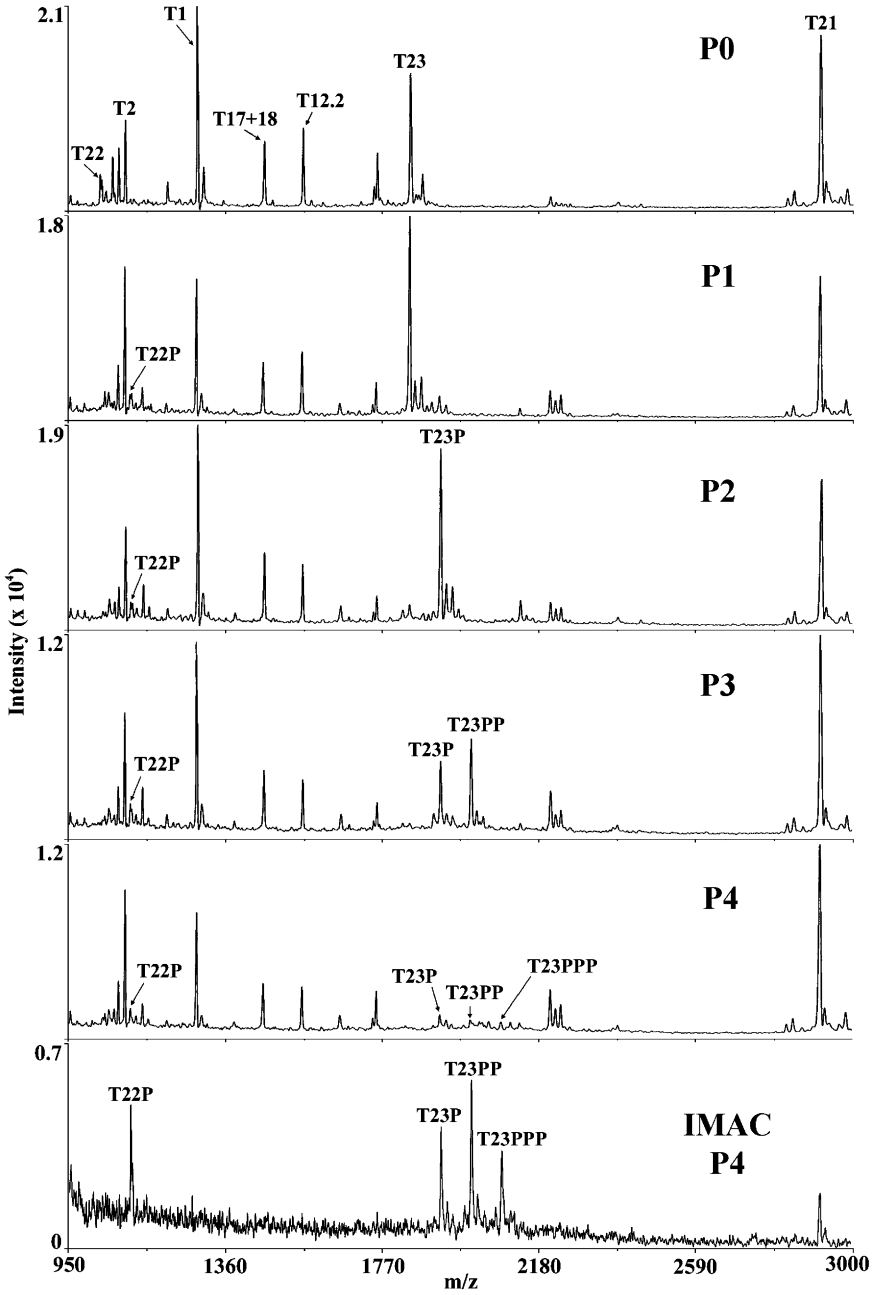

FIGURE 5: MALDI MS analysis of the in-gel tryptic digests of P0−P4 21 kDa spots. Tryptic digests of spectrin P1−P4 and β16−17C P0 were analyzed in linear mode with delayed extraction. The peaks corresponding to tryptic peptides of the 21 kDa C-terminal fragment are indicated. MALDI MS analysis of phosphorylated peptides eluted from an IMAC tip is shown for a tryptic digest of P4 (bottom spectrum).

phosphorylated. The y5−y7 ions indicate that Ser-2117 and -2120 were not phosphorylated, and the $y8^{\Delta}$ fragment, where Ser-2114 has been converted to dehydroalanine, allowed assignment of phosphorylation at Ser-2114. Interestingly, another intense ion at *m*/*z* 486.0 that does not correspond to any b or y ions was observed. This ion is 22 Da less than *m*/*z* 508.0 and was also produced when *m*/*z* 508.0 was subjected to subfragmentation (MS^3, data not shown). Subfragmentation of *m*/*z* 486.0 revealed that Thr-2113 of this ion had lost its side chain [$(H_3C)C(OH)$] (data not shown).

Similarly, MS/MS fragmentations of the doubly charged T23P (*m*/*z* 962.45) in P2, T23PP (*m*/*z* 1002.63) in P3, and T23PPP (*m*/*z* 1042.40) in P4 indicated that the second, third, and fourth phosphorylation events occurred on Ser-2125, Ser-2123, and Ser-2128, respectively (Figure 6). Analysis of P5 and P6 tryptic digests revealed a doubly charged *m*/*z* 596.78 and a triply charged *m*/*z* 999.43, corresponding to the calculated MH^+ of doubly phosphorylated T22 (T22PP) and singly phosphorylated T21 (T21P), respectively (Table 2). Examination of the b and y fragment ions allowed assignment of phosphorylation at Ser-2117 and Thr-2110, respectively (Figure 6). Tryptic digests of P7 and P8 were also analyzed by LC-MS/MS but no additional phosphorylation events were found. Therefore, LC-MS/MS successfully identified all the phosphorylated residues in charge states P1−P6 (Table 2). Figure 7 shows all the identified phosphorylation sites and the order of the phosphorylation events in β-spectrin. The locations of the phosphorylated residues in T22P and T23P were also confirmed by Edman sequencing of the appropriate RP-HPLC fractions (data not shown).

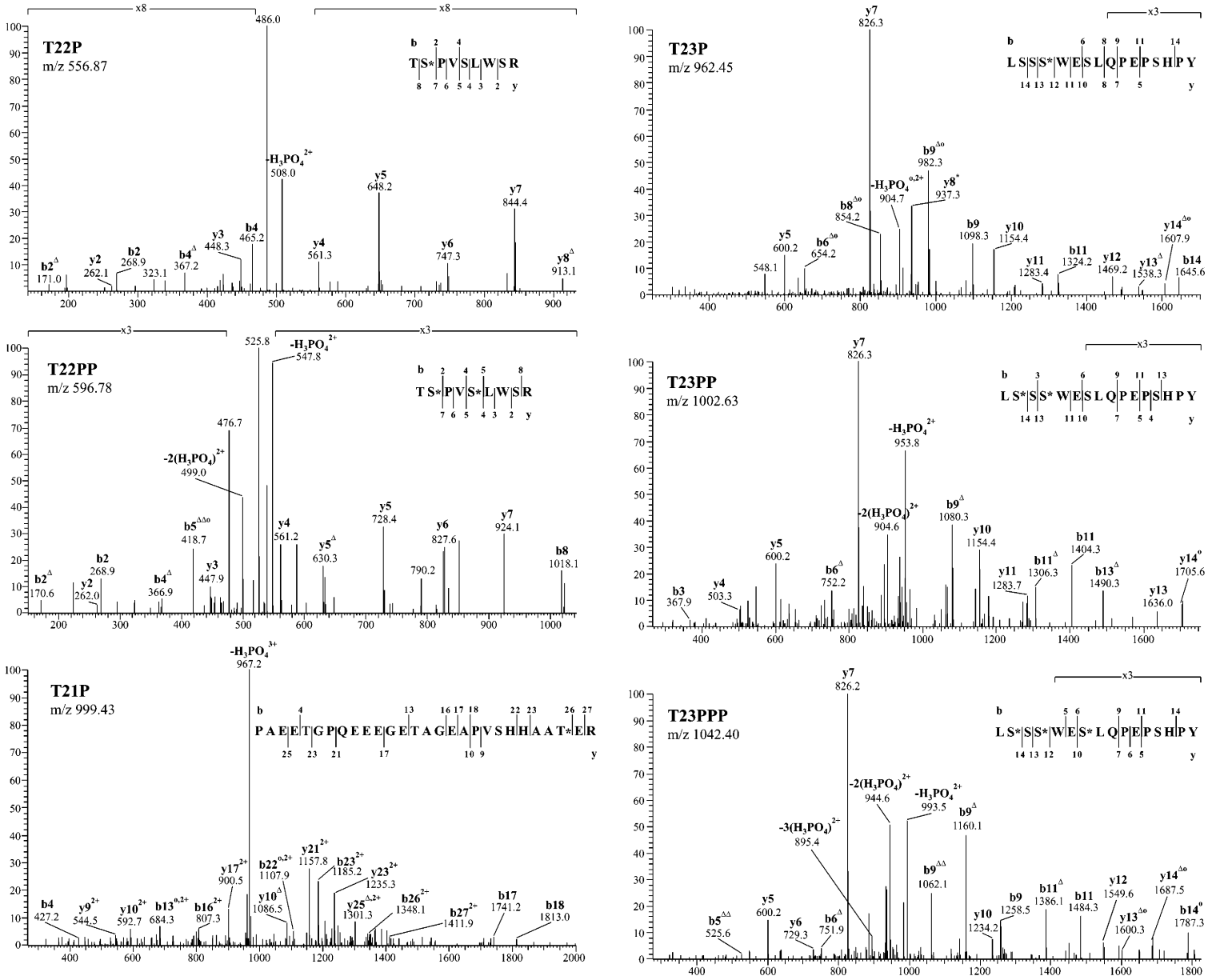

FIGURE 6: Tandem MS analysis of phosphorylated T21, T22, and T23 peptides. MS/MS spectra of the doubly charged *m*/*z* 962.45 (T23P), *m*/*z* 1002.63 (T23PP), *m*/*z* 1042.40 (T23PPP), *m*/*z* 556.87 (T22P), and *m*/*z* 596.78 (T22PP) and the triply charged *m*/*z* 999.43 (T21P) are shown. The phosphorylated residues are indicated by asterisks in the peptide sequences. The b and y fragment ions provide sequence information from the N- and C-termini, respectively. (△) fragment ions with a loss of 98 Da (H_3PO_4); (*) loss of 17 Da (NH_3); (○) loss of 18 Da (H_2O). (2+) and (3+) indicate doubly- and triply-charged ions, respectively.

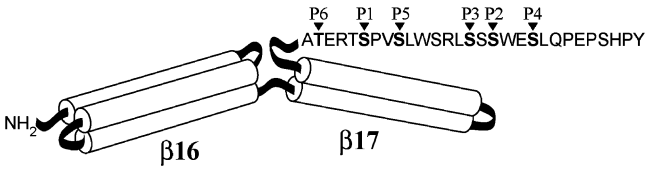

FIGURE 7: Model showing the six phosphorylation sites of β-spectrin. The last two homologous motifs and the nonhomologous C-terminal region of β-spectrin are shown. The 16th motif contains the complete three helices, whereas the 17th motif has only two helices. Immediately after the partial 17th motif is the phosphorylated nonhomologous C-terminal region. The six phosphorylation sites (indicated by arrowheads) and the sequential phosphorylation events (P1− P6) are as shown.

DISCUSSION

Spectrin is a major component of the membrane skeleton that is phosphorylated, but the role of phosphorylation is poorly understood due to the lack of detailed understanding of the phosphorylation events occurring in vivo. In this study, we exploited the fact that phosphorylation of a protein changes its isoelectric point to distinguish the unphosphorylated and multiple phosphorylated spectrin NTCB peptides on 2-D gels. Separation of phosphorylated spectrin NTCB peptides by 2-DE has been attempted previously (*6*, *40*), and up to six charge states have been reported (*40*). However, no structural analysis was performed on these charge-shifted spots, and these older 2-DE methods did not provide sufficient separation of the phosphorylated peptides. Furthermore, visualization of the charge states by autoradiographic detection of ^{32}P-labeled phosphopeptides (*40*) did not permit accurate quantitation of the various charge states because the method only measures phosphorylation turnover and not basal levels.

We used peptide isolation and characterization methods to elucidate the major β-spectrin phosphorylation sites. Using our improved procedures, we observed a total of nine charge states (P0−P8) for the 21 and 32 kDa β-spectrin NTCB fragments. The most basic component (P0) of the 21 kDa fragments was unambiguously determined as the unphosphorylated peptide by use of NTCB-cleaved recombinant β16−17C from *Escherichia coli* as a reference. The eight components more acidic than P0 suggest the presence of up to eight phosphorylation sites. Most β-spectrin proteins isolated from fresh blood exist in the lower phosphorylation states (P1−P4); only 1.5% are unphosphorylated, and 9.3% have more than four phosphorylations. The low amount of the higher phosphorylation states observed is not due to the inability of Sp316 to recognize these phosphorylated peptides, since the higher phosphorylation sites are quite far from the antibody's epitope, at least in the linear sequence. In addition, ^{32}P-phosphate-labeled spectrin NTCB peptides displayed lesser amounts of the higher phosphorylation states when analyzed on 2-D gels (data not shown; *40*). It is also unlikely that the highly phosphorylated proteins were tightly bound to the membrane and not extractable by the method employed because it was reported that spectrin isolated by direct lysis of ^{32}P-labeled erythrocytes in 5% SDS at 100 °C contained identical specific activity as purified spectrin dimer (*53*). The identical specific activities observed also indicate that no significant dephosphorylation occurred during the purification of spectrin dimer (*53*). Supporting this, we observed similar phosphorylation patterns when spectrin was prepared in the presence of phosphatase inhibitors (sodium fluoride and sodium orthovanadate; data not shown). Therefore, aside from minor non-phosphate-related charge shifts (see below), the phosphorylation pattern observed on 2-D gels closely reflects the phosphorylation status of spectrin in vivo.

Although the side reactions caused by NTCB had been greatly reduced, we could still detect a minor amount of charge heterogeneity on the 2-D gel analysis of NTCB-cleaved β16−17C (Figure 3C) as well as β16−17C controls that were not exposed to NTCB. Typically, two acidic shifts were observed when ~100 μg of NTCB-cleaved β16−17C was analyzed. The nature of these charge shifts is unknown, but deamidation of asparagine and glutamine residues are likely possibilities (*54*, *55*). In addition, some degree of horizontal streaking was often observed on 2-DE. While the amount of streaking is minimal, it does contribute to the heterogeneity of neighboring spots. Due to non-phosphate-related charge shifts, it is very likely that not all the nine charge states observed are caused by phosphorylation. In support of this, only six phosphorylation sites have been identified by LC-MS/MS and no new phosphorylated peptides were observed in P7 and P8. This suggests that P7 and P8 are caused by non-phosphorylation charge shifts of P5 and P6. More importantly, on the basis of quantitation of 2-D gel spots, the six phosphorylation events identified in this study account for at least 96% of the spectrin molecules in freshly isolated human red cells. Therefore, even if P7 and P8 do exist, their very low level argues against a meaningful physiological role.

RP-HPLC and MALDI MS tryptic peptide mapping of the 2-D gel spots clearly showed that the phosphorylation of β-spectrin progressed through a distinctive ordered mechanism. The first four phosphorylations (P1−P4) occurred on T22, T23, T23P, and T23PP, respectively. Each site appeared to be completely phosphorylated before the next phosphorylation occurred. Of course, due to the non-phosphate-related charge shifts, some minor mixing of the phosphorylation states was observed. The phosphorylation states of P5 and P6 were more complicated as the low amount of these two components was greatly influenced by charge shifts from the abundant lower-phosphorylation states. Therefore, the acidic shift of P3 and P4 to P5 resulted in a substantial amount of T22P in P5. For this reason, phosphorylation of T22P predominates in P5. Similarly, charge shifts from P4 and P5 affected the P6 phosphorylation state. However, the decrease in T21 peak and the ability to detect phosphorylated T21 by LC-MS/MS allowed us to assign phosphorylation of T21 as the P6 phosphorylation state. The sequential phosphorylation of spectrin suggests that each phosphorylation event may induce a conformational change that exposes the next available site. Alternatively, the phosphorylated residue may serve as part of the kinase(s) recognition site for the next phosphorylation event.

The phosphorylated region of β-spectrin has previously been localized to the last three tryptic peptides of the protein with a combined mass of 10.5 kDa by use of older protein chemical methods prior to the availability of mass spectrometry (*19*). Since the calculated mass of the nonhomologous C-terminal region of β-spectrin is only 5.8 kDa, the phosphorylated region might extend into the tetramerization domain of β-spectrin. In this report, six phosphorylation sites

have been identified by tandem MS. Five of the phosphorylations occur on serine residues and one on threonine. Surprisingly, only a minor amount of phosphothreonine was detected, compared to the approximately 25% phosphothreonine originally reported by Harris and Lux (*19*). All the identified phosphorylated residues are located on tryptic peptides T21, T22, and T23, which are all on the nonhomologous C-terminal region of β-spectrin (Figure 7). The adjacent tryptic peptides containing phosphorylatable residues on β17 motif (T16 and T17+18) did not show any significant variation on the RP-HPLC maps (Figure 4). Therefore, there is no evidence that phosphorylation extends into the tetramerization region of β-spectrin. In addition, in an earlier study (*9*) we analyzed mild tryptic digests of spectrin by 2-DE and identified a 17 kDa β-spectrin peptide (spot 2001) involved in head-to-head $\alpha\beta$ association, which contained the entire β17 motif and did not display any charge shift indicative of phosphorylation. Therefore, we conclude that no detectable phosphorylation occurs outside the C-terminal nonhomologous region of β-spectrin (T21−T23).

In summary, this study has identified the precise sites of all significant phosphorylation events on β-spectrin and determined that these phosphorylation events apparently occur in a tightly regulated sequential order. With knowledge of the phosphorylation pattern of β-spectrin, it will now be possible to correlate spectrin phosphorylation events with changes to membrane/spectrin properties in future in vivo as well as recombinant protein studies.

ACKNOWLEDGMENT

We gratefully acknowledge the Wistar Institute Monoclonal Antibody Core Facility for assistance in producing the Sp316 monoclonal antibody. We thank Sophie Pedroni, Curtis Lawrence, and Chad Grabner for contributions to preliminary work that led to this study and Sandy Harper for helpful comments on the manuscript.

REFERENCES

1. Bennett, V. (1985) The membrane skeleton of human erythrocytes and its implications for more complex cells, *Annu. Rev. Biochem. 54*, 273−304.
2. Marchesi, V. T. (1985) Stabilizing infrastructure of cell membranes, *Annu. Rev. Cell. Biol. 1*, 531−561.
3. Mohandas, N., and Chasis, J. A. (1993) Red blood cell deformability, membrane material properties and shape: regulation by transmembrane, skeletal and cytosolic proteins and lipids, *Semin. Hematol. 30*, 171−192.
4. Sahr, K. E., Laurila, P., Kotula, L., Scarpa, A. L., Coupal, E., Leto, T. L., Linnenbach, A. J., Winkelmann, J. C., Speicher, D. W., Marchesi, V. T., Curtis, P. J., and Forget, B. G. (1990) The complete cDNA and polypeptide sequences of human erythroid alpha-spectrin, *J. Biol. Chem. 265*, 4434−4443.
5. Winkelmann, J. C., Chang, J. G., Tse, W. T., Scarpa, A. L., Marchesi, V. T., and Forget, B. G. (1990) Full-length sequence of the cDNA for human erythroid β-spectrin, *J. Biol. Chem. 265*, 11827−11832.
6. Speicher, D. W., Morrow, J. S., Knowles, W. J., and Marchesi, V. T. (1982) A structural model of human erythrocyte spectrin. Alignment of chemical and functional domains, *J. Biol. Chem. 257*, 9093−9101.
7. Speicher, D. W., and Marchesi, V. T. (1984) Erythrocyte spectrin is comprised of many homologous triple helical segments, *Nature 311*, 177−180.
8. Tse, W. T., Lecomte, M. C., Costa, F. F., Garbarz, M., Feo, C., Boivin, P., Dhermy, D., and Forget, B. G. (1990) Point mutation in the β-spectrin gene associated with alpha I/74 hereditary elliptocytosis. Implications for the mechanism of spectrin dimer self-association, *J. Clin. Invest. 86*, 909−916.
9. Speicher, D. W., DeSilva, T. M., Speicher, K. D., Ursitti, J. A., Hembach, P., and Weglarz, L. (1993) Location of the human red cell spectrin tetramer binding site and detection of a related "closed" hairpin loop dimer using proteolytic footprinting, *J. Biol. Chem. 268*, 4227−4235.
10. Kennedy, S. P., Weed, S. A., Forget, B. G., and Morrow, J. S. (1994) A partial structural repeat forms the heterodimer self-association site of all β-spectrins, *J. Biol. Chem. 269*, 11400−11408.
11. Garbarz, M., Tse, W. T., Gallagher, P. G., Picat, C., Lecomte, M. C., Galibert, F., Dhermy, D., and Forget, B. G. (1991) Spectrin Rouen (β 220−218), a novel shortened β-chain variant in a kindred with hereditary elliptocytosis. Characterization of the molecular defect as exon skipping due to a splice site mutation, *J. Clin. Invest. 88*, 76−81.
12. Eber, S. W., Morris, S. A., Schroter, W., and Gratzer, W. B. (1988) Interactions of spectrin in hereditary elliptocytes containing truncated spectrin β-chains, *J. Clin. Invest. 81*, 523−530.
13. Tse, W. T., Gallagher, P. G., Pothier, B., Costa, F. F., Scarpa, A., Delaunay, J., and Forget, B. G. (1991) An insertional frameshift mutation of the β-spectrin gene associated with elliptocytosis in spectrin nice (β 220/216), *Blood 78*, 517−523.
14. Gallagher, P. G., Tse, W. T., Costa, F. F., Scarpa, A., Boivin, P., Delaunay, J., and Forget, B. G. (1991) A splice site mutation of the β-spectrin gene causing exon skipping in hereditary elliptocytosis associated with a truncated β-spectrin chain, *J. Biol. Chem. 266*, 15154−15159.
15. McGuire, M., and Agre, P. (1988) Clinical disorders of the erythrocyte membrane skeleton, *Hematol. Pathol. 2*, 1−14.
16. Palek, J., and Lambert, S. (1990) Genetics of the red cell membrane skeleton, *Semin. Hematol. 27*, 290−332.
17. Yoon, S. H., Yu, H., Eber, S., and Prchal, J. T. (1991) Molecular defect of truncated β-spectrin associated with hereditary elliptocytosis. β-spectrin Gottingen, *J. Biol. Chem. 266*, 8490−8494.
18. Lecomte, M. C., Gautero, H., Bournier, O., Galand, C., Lahary, A., Vannier, J. P., Garbarz, M., Delaunay, J., Tchernia, G., Boivin, P., and Dhermy, D. (1992) Elliptocytosis-associated spectrin Rouen (β 220/218) has a truncated but still phosphorylatable β chain, *Br. J. Haematol. 80*, 242−250.
19. Harris, H. W., Jr., and Lux, S. E. (1980) Structural characterization of the phosphorylation sites of human erythrocyte spectrin, *J. Biol. Chem. 255*, 11512−11520.
20. Trepanier, D. J., Thibert, R. J., Draisey, T. F., and Caines, P. S. (1996) Carbamylation of erythrocyte membrane proteins: an in vitro and in vivo study, *Clin. Biochem. 29*, 347−355.
21. Corsi, D., Galluzzi, L., Crinelli, R., and Magnani, M. (1995) Ubiquitin is conjugated to the cytoskeletal protein alpha-spectrin in mature erythrocytes, *J. Biol. Chem. 270*, 8928−8935.
22. Corsi, D., Galluzzi, L., Lecomte, M. C., and Magnani, M. (1997) Identification of alpha-spectrin domains susceptible to ubiquitination, *J. Biol. Chem. 272*, 2977−2983.
23. Resmi, H., Pekcetin, C., and Guner, G. (2001) Erythrocyte membrane and cytoskeletal protein glycation and oxidation in short-term diabetic rabbits, *Clin. Exp. Med. 1*, 187−193.
24. Schwartz, R. S., Madsen, J. W., Rybicki, A. C., and Nagel, R. L. (1991) Oxidation of spectrin and deformability defects in diabetic erythrocytes, *Diabetes 40*, 701−708.
25. Boivin, P., Garbarz, M., Dhermy, D., and Galand, C. (1981) In vitro phosphorylation of the red blood cell cytoskeleton complex by cyclic AMP-dependent protein kinase from erythrocyte membrane, *Biochim. Biophys. Acta 647*, 1−6.
26. Avruch, J., Fairbanks, G., and Crapo, L. M. (1976) Regulation of plasma membrane protein phosphorylation in two mammalian cell types, *J. Cell Physiol. 89*, 815−826.
27. Boivin, P. (1988) Role of the phosphorylation of red blood cell membrane proteins, *Biochem. J. 256*, 689−695.
28. Graham, C., Avruch, J., and Fairbanks, G. (1976) Phosphoprotein phosphatase of the human erythrocyte, *Biochem. Biophys. Res. Commun. 72*, 701−708.
29. Usui, H., Kinohara, N., Yoshikawa, K., Imazu, M., Imaoka, T., and Takeda, M. (1983) Phosphoprotein phosphatases in human erythrocyte cytosol, *J. Biol. Chem. 258*, 10455−10463.
30. Usui, H., Imazu, M., Maeta, K., Tsukamoto, H., Azuma, K., and Takeda, M. (1988) Three distinct forms of type 2A protein phosphatase in human erythrocyte cytosol, *J. Biol. Chem. 263*, 3752−3761.

31. Avruch, J., and Fairbanks, G. (1974) Phosphorylation of endogenous substrates by erythrocyte membrane protein kinases. I. A monovalent cation-stimulated reaction, *Biochemistry 13*, 5507−5514.
32. Hosey, M. M., and Tao, M. (1977) Phosphorylation of rabbit and human erythrocyte membranes by soluble adenosine 3′:5′-monophosphate-dependent and -independent protein kinases, *J. Biol. Chem. 252*, 102−109.
33. Wolfe, L. C., and Lux, S. E. (1978) Membrane protein phosphorylation of intact normal and hereditary spherocytic erythrocytes, *J. Biol. Chem. 253*, 3336−3342.
34. Ungewickell, E., and Gratzer, W. B. (1978) Self-association of human spectrin. A thermodynamic and kinetic study, *Eur. J. Biochem. 88*, 379−385.
35. Anderson, J. M., and Tyler, J. M. (1980) State of spectrin phosphorylation does not affect erythrocyte shape or spectrin binding to erythrocyte membranes, *J. Biol. Chem. 255*, 1259−1265.
36. Lu, P. W., Soong, C. J., and Tao, M. (1985) Phosphorylation of ankyrin decreases its affinity for spectrin tetramer, *J. Biol. Chem. 260*, 14958−14964.
37. Manno, S., Takakuwa, Y., Nagao, K., and Mohandas, N. (1995) Modulation of erythrocyte membrane mechanical function by β-spectrin phosphorylation and dephosphorylation, *J. Biol. Chem. 270*, 5659−5665.
38. Perrotta, S., del Giudice, E. M., Iolascon, A., De Vivo, M., Di Pinto, D., Cutillo, S., and Nobili, B. (2001) Reversible erythrocyte skeleton destabilization is modulated by β-spectrin phosphorylation in childhood leukemia, *Leukemia 15*, 440−444.
39. Anderson, J. M. (1979) Structural studies on human spectrin. Comparison of subunits and fragmentation of native spectrin, *J. Biol. Chem. 254*, 939−944.
40. Pedroni, S., Lecomte, M. C., Gautero, H., and Dhermy, D. (1993) Heterogeneous phosphorylation of erythrocyte spectrin β chain in intact cells, *Biochem. J. 294*, 841−846.
41. Wechsler, A., and Teichberg, V. I. (1998) Brain spectrin binding to the NMDA receptor is regulated by phosphorylation, calcium and calmodulin, *EMBO J. 17*, 3931−3939.
42. Speicher, D. W., Weglarz, L., and DeSilva, T. M. (1992) Properties of human red cell spectrin heterodimer (side-to-side) assembly and identification of an essential nucleation site, *J. Biol. Chem. 267*, 14775−14782.
43. Harper, S., and Speicher, D. W. (1997) Expression and purification of GST fusion proteins, in *Current Protocols in Protein Science* (Coligan, J. E., Dunn, B. M., Ploegh, H. L., Speicher, D. W., and Wingfield, P. T., Eds.) pp 6.6.1−6.6.21, John Wiley & Sons, New York.
44. Degani, Y., and Patchornik, A. (1974) Cyanylation of sulfhydryl groups by 2-nitro-5-thiocyanobenzoic acid. High-yield modification and cleavage of peptides at cysteine residues, *Biochemistry 13*, 1−11.
45. Laemmli, U. K. (1970) Cleavage of structural proteins during the assembly of the head of bacteriophage T4, *Nature 227*, 680−685.
46. Zuo, X., Echan, L., Hembach, P., Tang, H. Y., Speicher, K. D., Santoli, D., and Speicher, D. W. (2001) Towards global analysis of mammalian proteomes using sample prefractionation prior to narrow pH range two-dimensional gels and using one-dimensional gels for insoluble and large proteins, *Electrophoresis 22*, 1603−1615.
47. Speicher, K. D., Kolbas, O., Harper, S., and Speicher, D. W. (2000) Systematic analysis of peptide recoveries from in-gel digestions for femtomole protein identifications in proteome studies, *J. Biomol. Technol. 11*, 74−86.
48. Shevchenko, A., Wilm, M., Vorm, O., and Mann, M. (1996) Mass spectrometric sequencing of proteins silver-stained polyacrylamide gels, *Anal. Chem. 68*, 850−858.
49. Gianazza, E. (1995) Isoelectric focusing as a tool for the investigation of posttranslational processing and chemical modifications of proteins, *J. Chromatogr. A 705*, 67−87.
50. Posewitz, M. C., and Tempst, P. (1999) Immobilized gallium(III) affinity chromatography of phosphopeptides, *Anal. Chem. 71*, 2883−2892.
51. DeGnore, J. P., and Qin, J. (1998) Fragmentation of phosphopeptides in an ion trap mass spectrometer, *J. Am. Soc. Mass Spectrom. 9*, 1175−1188.
52. Ogueta, S., Rogado, R., Marina, A., Moreno, F., Redondo, J. M., and Vazquez, J. (2000) Identification of phosphorylation sites in proteins by nanospray quadrupole ion trap mass spectrometry, *J. Mass Spectrom. 35*, 556−565.
53. Harris, H. W., Jr., Levin, N., and Lux, S. E. (1980) Comparison of the phosphorylation of human erythrocyte spectrin in the intact red cell and in various cell-free systems, *J. Biol. Chem. 255*, 11521−11525.
54. Geiger, T., and Clarke, S. (1987) Deamidation, isomerization, and racemization at asparaginyl and aspartyl residues in peptides. Succinimide-linked reactions that contribute to protein degradation, *J. Biol. Chem. 262*, 785−794.
55. Robinson, N. E., and Robinson, A. B. (2001) Deamidation of human proteins, *Proc. Natl. Acad. Sci. U.S.A. 98*, 12409−12413.

BI036092X